Article

Early-Stage Temperature Gradients in Glazed Spandrels Due to Aesthetical Features to Support Design for Thermal Shock

Jacopo Montali [1,*] **, Luciano Laffranchini** [2] **and Carlo Micono** [2]

[1] Algorixon, 43125 Parma, Italy
[2] Ai Studio, 10128 Turin, Italy; llaffranchini@aigroup.it (L.L); cmicono@aigroup.it (C.M.)
[*] Correspondence: jacopo@algorixon.com

Abstract: Investigating thermal breakage of glass panes requires careful analysis of the environmental boundary conditions to determine the expected thermal gradient between the sunlit and shaded parts of the glass. This is particularly critical for glazed spandrels, where an opaque posterior insulation layer normally increases the system's temperatures. The choice of the spandrel system should also be evaluated against the aesthetical impression that it conveys. The aim of this study is to understand how early design factors, such as aesthetical features like color, are driving temperature gradients in the glazed pane to design for thermal shock. Multiple finite-differences analyses in a quasi-static regime for non-ventilated, single glazed spandrels were conducted in three locations (London, New York and Mumbai). Results were then analyzed via a general linear model in SAS 9.4 and Tuckey post hoc analysis. It was shown that a low absorptance of the back insulation (e.g., light color) can lead to a wide range of possible temperature gradients depending on the glass transparency, with higher values of the thermally induced temperature gradients for more opaque glasses. Conversely, a high absorptance of the insulation layer leads to moderate values of glass temperature gradients, which are not substantially sensitive to the effect of the glass transparency.

Keywords: thermal shock; glass temperature; spandrel; early-stage design; façade design

1. Introduction

In recent years, the design of façades has become a complex decision-making process characterized by a multiplicity of stakeholders, intricacies and key decision points along the design process [1–4]. The early-stage selection of aesthetical features in glazed spandrels are an example of how decisions taken at conceptual stage affect following stages. Given the combined presence of insulation, glass and polymeric materials (e.g., interlayers, gaskets), and external solar radiation, temperatures in spandrel elements tend to increase significantly. Exceedingly elevated temperatures can lead to potential failures such as polyvinyl butyral (PVB) delamination, excessive temperatures in polymeric gaskets and, lastly, thermal shock in the glazed layer.

Current research on spandrels is mainly focusing on performance of finished products, rather than on providing approaches that can effectively support the early design of the system. The effect of surface treatment like fritting on the structural resistance [5] or condensation risk [6] has been studied. There are examples of temperature of real-world spandrel systems monitored over time [7] also to understand specific spandrel failures [8]. Other research strands performed parametric studies on the incidence of early-stage design parameters on energy consumption [9–11], on many design criteria concurrently [12,13] or, at a smaller scale, on the influence of design parameters on the expected performance of specific materials [14]. In the domain of opaque façades, parametric studies

have been conducted to understand the impact of aesthetical features on the expected performance. Widiastuti et al. [15,16] measured the influence of leaves density on a green façade on energy transfer. Tarabieh et al. [17] used the "hotbox" method to measure the U-value of different wall types in Egypt. However, there is no specific work aiming to provide design support for the specification of spandrels, although spandrels play a fundamental role in potential operational failures of the entire façade of buildings.

The present paper investigates how the spandrel system's basic aesthetical features induce temperature gradients in glazed spandrels to facilitate the early specification of system's thermo-physical properties against thermal shock. The analyses conducted in this paper explored different combinations of insulation, glass types for different locations, orientations and external shading to understand the key design drivers for the problem at hand. Inference over the generated data was then made by means of statistical analysis. Section 2 introduces the materials and methodology, whereas Sections 3–5 will present results, discussion and conclusion.

2. Materials and Methods

2.1. Materials

2.1.1. Spandrel Build-Up

A commonly used spandrel build-up was chosen as the base configuration to be analyzed (Figure 1). The build-up consists of a 150 mm rockwool insulation ($\lambda = 0.035$ W/mK), 6mm air cavity ($\lambda = 0.26$ W/mK) and a 66.2 (12.76 mm) laminated glass. The configuration shown in Figure 1 was then varied by changing those thermo-physical parameters that governed the aesthetics of the spandrel and the glass, such as the exterior insulation color and the transparency of the glass.
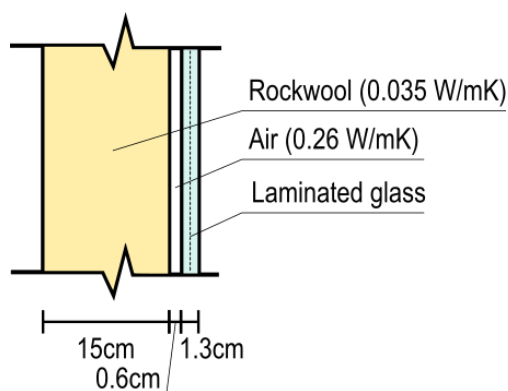
Figure 1. Build-up of analyzed spandrel.

Table 1 shows the chosen variations on the insulation types. It can be seen that the absorptance is the only factor that varies. This is motivated by the fact that the thermal resistance of the insulation, which arises from the combination of the material's thermal conductivity and thickness, does not affect the problem significantly (Appendix A). The color of external insulation is instead driving the effective absorptances of the whole system, thus playing a major role in the heat exchange between the different layers of the spandrel system. Since spandrels generally consist of sandwich panels made from an insulated core and two steel face sheets with low-emissivity properties, the emissivity for radiative exchange calculations was assumed to be fixed (0.02).

Table 1. Thermo-physical properties for the analyzed insulation.

Insulation Code	Description	Absorptance (-)	Emissivity (-)	Thermal Conductivity (W/mK)	Thickness (cm)
A1	Light color	0.20	0.02	0.035	15
A2	Medium color	0.55	0.02	0.035	15
A3	Dark color	0.90	0.02	0.035	15

The thermo-physical properties of the laminated glass were chosen for different solar absorptances (Table 2). Clear (G1), coated (G2) and fritted (G3) glass panes were chosen. All the selected glass panes have standard emissivity values (0.84) except for glass G2, whose internal coating reduces the emissivity towards the interior to 0.30.

Table 2. Thermo-physical properties for the analyzed single glazing.

Insulation Code	Description	Solar Transmittance (-)	Solar Absorptance (-)	Emissivity towards Interior (-)	Emissivity towards Exterior (-)
G1	Very transparent	0.81	0.12	0.84	0.84
G2	Semi-transparent	0.63	0.29	0.30	0.84
G3	Nearly opaque	0.36	0.59	0.84	0.84

2.1.2. Environmental Conditions

The analyses were conducted for three different climates. The environmental conditions were chosen for three urban areas based on different conditions of irradiance/maximum temperature/minimum temperature. Table 3 shows the main climatic data of the chosen locations.

Table 3. General environmental data for the three cities under analysis.

Location	Typical Meteorological Year	Latitude/Longitude	Maximum Global Irradiance on the Horizontal (W/m²)	Maximum External Temperature (°C)	Minimum External Temperature (°C)
London	Kew EWY	51°34′ N–0°11′ W	952.6	26.6	−6.1
New York	New York TMY2	40° 42′ N–74° 0′ O	1038.5	35.0	−15.6
Mumbai	Mumbai IWEC	19°04′ N–72°52′ E	1011.9	40.0	12.4

External heat exchange coefficients were assumed to be fixed and equal to 13 W/m²K for the summer season and 11 W/m²K otherwise as in [18]. These heat exchange coefficients assume absence of local wind on the external surface. Internal temperature equals 20°C in winter and 26 °C in spring, autumn and summer, whereas the internal heat exchange coefficient equals 7.7 W/m²K.
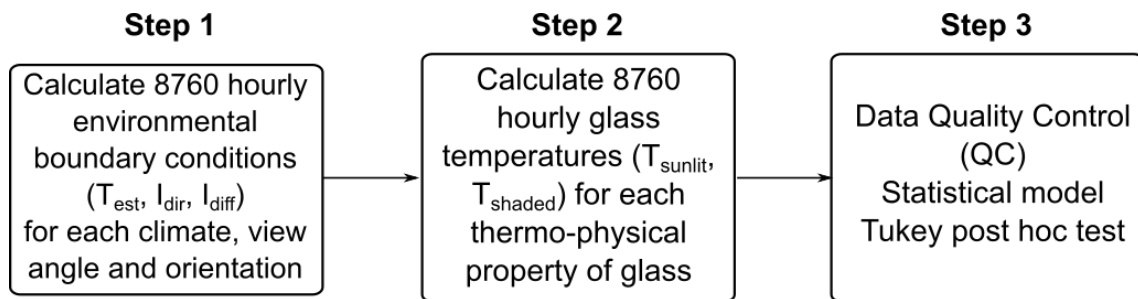
2.2. Methods

The thermally induced stresses that cause thermal breakage in the glass pane arise from the difference in temperature ΔT between the sunlit part of the glass T_{sunlit} and the shaded part T_{shaded}. The relevant thermal stress σ is calculated as:

$$\sigma = k_t \cdot E \cdot \alpha \cdot \Delta T \tag{1}$$

where k_t depends on the frame thermal inertia and the presence of drop shadow and can be taken to be equal to 1.1 as in [18]; E is the elastic modulus of the glass equal to 70 GPa; α is the linear expansion coefficient equal to 6×10^{-6} K^{-1}, and ΔT is the above-mentioned temperature differential.

The temperature gradient ΔT between the sunlit and shaded parts of a glass was calculated in the first two steps of the process map shown in Figure 2. Step 1 determined the 8760 hourly values of environmental boundary conditions (T_{est}, I_{dir}, I_{diff}) for each parameter shown in Table 4. Step 2 then determined the values of T_{sunlit}, and of T_{shaded}, for each possible combination of insulation/glass types

shown in Tables 1 and 2. Overall, 2,128,680 temperature gradients ΔT were generated. Step 3 involved data analysis as described in 2.2.3.

Step 1	Step 2	Step 3
Calculate 8760 hourly environmental boundary conditions (T_{est}, I_{dir}, I_{diff}) for each climate, view angle and orientation	Calculate 8760 hourly glass temperatures (T_{sunlit}, T_{shaded}) for each thermo-physical property of glass	Data Quality Control (QC) Statistical model Tukey post hoc test

Figure 2. Three-step process for the calculation of the temperature gradient in glasses.

Table 4. View angles (°) and orientations analyzed for each location.

| Location	View Angles Analyzed (°)	Orientations Analyzed
London	0-30-60	E-S-W
New York	0-30-60	E-S-W
Mumbai	0-30-60	E-S-W

2.2.1. Step 1: Hourly Environmental Conditions

The environmental boundary conditions for the problem were determined by running a number of energy models in Integrated Environmental Solutions Virtual Environment (IESVE) 2015 as in Figure 3. The models consisted of three rooms with different external building configurations providing shading in accordance with the view angles listed in Table 4 and as shown in Figure 4. The view angle measures the level of shading that the investigated point receives from front-facing buildings. Three orientations (East, South, West) were analyzed.

(a)   (b)   (c)
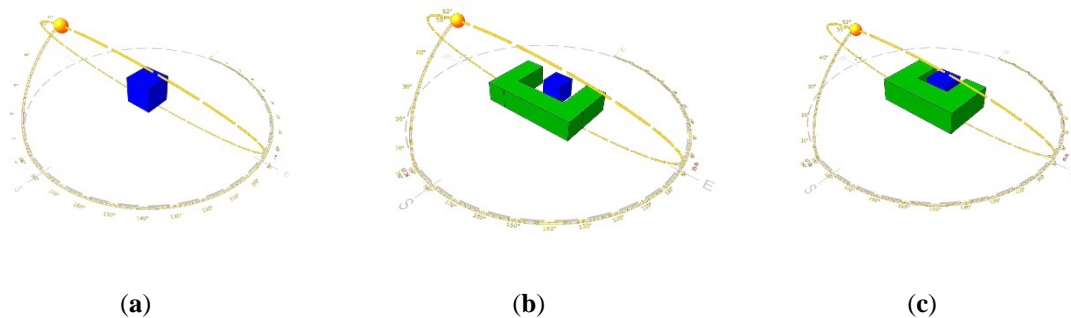
Figure 3. IES VE models generated for different view angles (**a**) 0°, (**b**) 30°, (**c**) 60°.
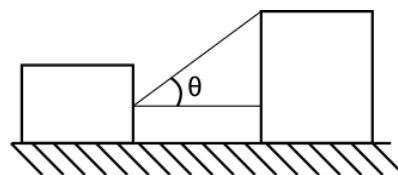
Figure 4. View angle to identify the presence of external obstructions limiting the solar radiation.

Overall, 236,520 hourly values of environmental boundary conditions (T_{est}, I_{dir}, I_{diff}) were found.

2.2.2. Step 2: Hourly Glass Temperatures

The above-mentioned boundary conditions were then used to solve the steady state (i.e., no heat storage), 1-D heat transfer problem for a multi-layered system with a modified version of Fourier's law by adding the convective and radiative heat exchange between adjacent layers:

$$\alpha_{ie}\Phi_s = \sum_j h_{c,ij}(T_i - T_j) + \sum_k h_{r,ij}(T_i - T_k) + \sum_l (\lambda/s)_{il}(T_i - T_l) \tag{2}$$

The left-hand side of (2) corresponds to the internal heat generation, represented as the product between the incident radiation Φ_s and the effective absorptance α_{ie} of the ith layer. The incident radiation equals the sum of the direct and the diffuse components, or the diffuse component only, depending on whether T_{sunlit} or T_{shaded} is sought. The right-hand side of (2) represents the heat exchange between layers. The coefficients $h_{c,ij}$ and $h_{r,ij}$ represent the convective and radiative heat exchanges between the analyzed ith layer and the adjacent layers j (for convective exchange) and k (for radiative exchange). The ratio $(\lambda/s)_{il}$ represents the conduction exchange between the ith layer under analysis and the lth adjacent layer. Temperatures T_i, T_j, T_k and T_l represent the temperature of the ith layer under analysis, the jth adjacent layer to the ith layer for convective exchange, the kth adjacent layer to the ith layer for radiative exchange and the lth adjacent layer to the ith layer for conduction exchange.

The generated thermal network for the problem is shown in Figure 5. $h_{con,cav}$ and $h_{rad,cav}$ are the convective and radiative conductances of the air cavity and they are defined in [19]. The former was defined as:

$$h_{con,cav} = Nu \frac{\lambda_{air}}{t_{air}} \tag{3}$$

$$Nu = A(Gr \cdot Pr)^n \tag{4}$$

$$Gr = \frac{9.81 \, t_{air}^3 \, \Delta T \, \rho_{air}}{T_m \mu_{air}^2} \tag{5}$$

$$Pr = \frac{\mu_{air} c_{air}}{\lambda_{air}} \tag{6}$$

where Nu is the Nusselt number, Gr is the Grashof number, Pr is the Prandtl number, λ_{air} is the thermal conductivity of still air (equal to 0.26 W/mK), t_{air} is the thickness of air (equal to 0.6 cm as shown in Figure 1), A and n are constants equal to 0.035 and 0.38, ΔT and T_m are the temperature gradient and the average temperature of the surfaces bounding the air gap, ρ_{air} is the density of air equal to 1.18 kg/m^3, μ_{air} is the dynamic viscosity of air equal to 1.85×10^{-5} kg/ms, and c_{air} is the specific heat capacity of air equal to 1005 J/kgK. The radiative air conductance is defined as:

$$h_{rad,cav} = 4\sigma \left(\frac{1}{\varepsilon_1} + \frac{1}{\varepsilon_2} - 1 \right)^{-1} T_m^3 \tag{7}$$

where σ is the Stephan–Boltzmann constant (5.67×10^{-8} W/m^{2}K^4), and ε_1 and ε_2 are the emissivities of the surfaces, equal to 0.02 and 0.89.
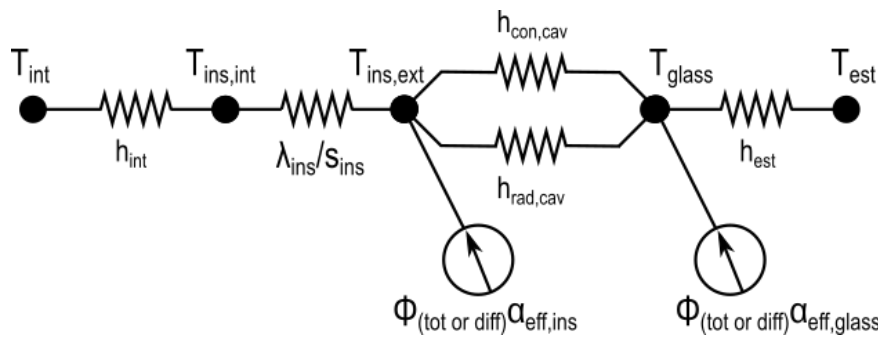
Figure 5. Thermal network generated from the local analysis of the spandrel system shown in Figure 1.

Equation (2) generated a system of equations of the type $A\underline{T} = \underline{b}$, where A is the coefficient matrix, $\underline{b}$ is a constant vector, and $\underline{T}$ is the solution for the problem. Once A and $\underline{b}$ are found, the solution $\underline{T}$ is equal to $\underline{T} = A^{-1}\underline{b}$. Since internal heat exchange coefficients varied with temperature, $A = A(\underline{T}) \neq const$. Thus, the solution was found iteratively until the value of the error e is less than 0.05K, where e is defined as:

$$e = \sum_i (T_{i,t+1} - T_{i,t}) \tag{8}$$

where t represents the instant under analysis. The effective absorptance of the ith layer α_{ie} is such that:

$$\alpha_{tot} = \sum_i \alpha_{ie} \tag{9}$$

where α_{tot} is the total absorptance of the system, including opaque components positioned behind the glazed system (like in a spandrel system). In general, $\alpha_{tot} \neq \alpha_{glass}$, where α_{glass} is the value normally provided by the glass manufacturer. Thus, α_{ie} is the ratio of the solar radiation that is absorbed by the ith component. This value was calculated from an additional system of equations describing the balance of the radiative fluxes between the layers of the system, when the external solar radiation is unity ($\Phi_s = 1$). The fluxes in each layer were divided into reflected, transmitted and absorbed. Thus, under the hypothesis that the surrounding environment was totally absorptant, the following three equations were written for each layer:

$$\Phi_{i,i+1} = \tau_{i,1} \cdot \Phi_{i-1,i} + \rho_{i,2} \cdot \Phi_{i+1,i} \tag{10}$$

$$\Phi_{i,i-1} = \rho_{i,1} \cdot \Phi_{i-1,i} + \tau_{i,2} \cdot \Phi_{i+1,i} \tag{11}$$

$$\Phi_{i,i} = \alpha_{i,1} \cdot \Phi_{i-1,i} + \alpha_{i,2} \cdot \Phi_{i+1,i} \tag{12}$$

where the subscripts $i - 1$, i and $i + 1$ refer to the radiative fluxes from the ith component towards the exterior, absorbed by the ith component and towards the interior. The subscript 1 and 2 refer to radiative properties towards the exterior and the interior. $\Phi_{i,i}$ is the effective absorptance of the ith component ($\Phi_{i,i} = \alpha_{ie}$) and it was included into the left-hand side of Equation (2).

Analyses were conducted for both total ($\Phi_{tot} = \Phi_{diff} + \Phi_{dir}$) and diffuse ($\Phi_{diff}$) radiations to determine T_{sunlit} and T_{shaded}, respectively. The temperature gradient ΔT was calculated as T_{sunlit}-T_{shaded}.

2.2.3. Step 3: Data Analysis

The quality of the generated data (QC) was first checked in SAS 9.4 [20] by looking for missing values, outliers and distribution normality. The interaction between glass transparency and insulation absorptance to determine temperature gradients at extreme irradiance conditions was then analyzed. Quartile classes of irradiance were first calculated at each location; then, the 4th quartile was further

subdivided into quartiles, and the 4th quartile of the latter set was taken to consider the most extreme cases. The extreme case was then the value corresponding to a 6.25% probability of being exceeded. The irradiances corresponding to these values were above 404 W/m^2 in Mumbai, above 326 W/m^2 in London and above 397 W/m^2 in New York.

The chosen statistical model considered the interaction between glass transparency and insulation absorptance, and it was defined as:

$$y_{ij} = \mu + glass\_transparency_i \cdot insulation\_absorptance_j + e_{ij} \tag{13}$$

where y_{ij} is the observed temperature gradient, μ is the mean temperature gradient at each location; the product of glass_transparency$_i$ and insulation_absorptance$_j$ represents the fixed effect of the interaction between the ith level of glass transparency ($i = [0.4,0.6,0.8]$) and the jth level of absorptance insultation ($j = [0.2,0.6,0.9]$); and e_{ij} is the random residual effect $e_{ij} \sim N(0, \sigma_e^2)$.

The Tuckey post hoc test was then applied to evaluate the differences across locations per each level of interaction between glass transparency and absorbance insultation. This statistical analysis aimed to (1) estimate differences for all pairwise comparisons and (2) adjust the *p*-values for multiple testing and evaluate least square mean (LSM) differences. Differences were declared significant if *p*-value < 0.05 and results were reported as LSM.

3. Results

In total, 243 (3 locations, 3 orientations, 3 view factors, 3 glass types and 3 insulation colors) simulations were run on a Dell Inspiron laptop with an Intel Core i7 processor at 2.40GHz. The overall calculation time was 34.3 h. The generated data can be found in the Supplementary Materials (Tables S1–S3) that accompanies this paper. The results can be used by designers to swiftly acquire a better understanding of how design choices can affect thermal shock risk and the expected temperature differential as a function of the principal visual features of the spandrel element.

3.1. Maximum Temperature Gradients and Relevant Thermal Stresses

Each simulation determined 8760 hourly data in which the temperature gradient was defined. Tables 5–10 show the maximum values of temperature gradient for the three climates analyzed and the relevant thermally induced stress. Each table defines values for a specific combination of the analyzed variables. The values of the thermo-physical properties of the glass have been adjusted to their descriptive values (description fields in Tables 1 and 2).

Table 5. Maximum temperature gradients (K) for New York.

		Exposition Type								
		South			East			West		
		View Angle θ			View Angle θ			View Angle θ		
Glass Type	Insulation Color	0°	30°	60°	0°	30°	60°	0°	30°	60°
Very transparent	Light	37	26	12	30	22	10	30	22	10
	Medium	34	24	11	28	21	10	28	21	9
	Dark	40	28	13	33	24	11	33	24	11
Semi-transparent	Light	49	34	16	41	30	14	41	30	13
	Medium	39	27	13	32	23	11	32	23	10
	Dark	41	29	13	34	25	12	34	25	11
Nearly opaque	Light	59	42	19	49	36	17	49	36	16
	Medium	45	31	15	37	27	13	37	27	12
	Dark	44	31	14	36	27	13	37	27	12

Table 6. Maximum thermal stresses (MPa) for New York.

		Exposition Type								
		South			East			West		
		View Angle θ			View Angle θ			View Angle θ		
Glass Type	**Insulation Color**	**0°**	**30°**	**60°**	**0°**	**30°**	**60°**	**0°**	**30°**	**60°**
Very transparent	Light	54	35	12	58	32	11	58	28	9
	Medium	50	32	11	54	30	11	54	26	9
	Dark	59	38	13	64	35	13	63	31	10
Semi-transparent	Light	72	47	16	78	43	15	77	38	13
	Medium	57	37	12	61	34	12	61	30	10
	Dark	60	39	13	65	36	13	65	31	11
Nearly opaque	Light	87	57	19	94	52	19	94	46	15
	Medium	66	43	14	71	39	14	71	34	12
	Dark	64	42	14	70	39	14	69	34	11

Table 7. Maximum temperature gradients (K) for London.

		Exposition Type								
		South			East			West		
		View Angle θ			View Angle θ			View Angle θ		
Glass Type	**Insulation Color**	**0°**	**30°**	**60°**	**0°**	**30°**	**60°**	**0°**	**30°**	**60°**
Very transparent	Light	54	35	12	58	32	11	58	28	9
	Medium	50	32	11	54	30	11	54	26	9
	Dark	59	38	13	64	35	13	63	31	10
Semi-transparent	Light	72	47	16	78	43	15	77	38	13
	Medium	57	37	12	61	34	12	61	30	10
	Dark	60	39	13	65	36	13	65	31	11
Nearly opaque	Light	87	57	19	94	52	19	94	46	15
	Medium	66	43	14	71	39	14	71	34	12
	Dark	64	42	14	70	39	14	69	34	11

Table 8. Maximum thermal stresses (MPa) for London.

		Exposition Type								
		South			East			West		
		View Angle θ			View Angle θ			View Angle θ		
Glass Type	**Insulation Color**	**0°**	**30°**	**60°**	**0°**	**30°**	**60°**	**0°**	**30°**	**60°**
Very transparent	Light	32	21	7	34	19	7	34	17	6
	Medium	30	19	6	32	18	6	32	15	5
	Dark	35	23	8	38	21	7	38	18	6
Semi-transparent	Light	43	28	9	46	26	9	46	22	8
	Medium	34	22	7	36	20	7	36	18	6
	Dark	36	23	8	39	21	8	38	19	6
Nearly opaque	Light	52	34	11	56	31	11	56	27	9
	Medium	39	25	8	42	23	8	42	20	7
	Dark	38	25	8	41	23	8	41	20	7

Table 9. Maximum temperature gradients (K) for Mumbai.

		Exposition Type								
		South			East			West		
		View Angle θ			View Angle θ			View Angle θ		
Glass Type	**Insulation Color**	**0°**	**30°**	**60°**	**0°**	**30°**	**60°**	**0°**	**30°**	**60°**
Very transparent	Light	43	40	18	37	29	13	40	31	14
	Medium	40	37	16	35	27	12	37	29	13
	Dark	48	43	19	41	32	14	44	34	15
Semi-transparent	Light	58	53	24	50	39	17	53	42	19
	Medium	46	42	19	39	31	14	42	33	15
	Dark	49	44	20	42	33	14	45	35	16
Nearly opaque	Light	70	64	29	61	48	21	65	50	23
	Medium	53	49	22	46	36	16	49	38	17
	Dark	52	48	21	45	35	16	48	37	17

Table 10. Maximum thermal stresses (MPa) for Mumbai.

		Exposition Type								
		South			East			West		
		View Angle θ			View Angle θ			View Angle θ		
Glass Type	**Insulation Color**	**0°**	**30°**	**60°**	**0°**	**30°**	**60°**	**0°**	**30°**	**60°**
Very transparent	Light	26	24	10	22	17	8	24	18	8
	Medium	24	22	10	21	16	7	22	17	8
	Dark	28	26	11	24	19	8	26	20	9
Semi-transparent	Light	34	32	14	30	23	10	32	25	11
	Medium	27	25	11	23	18	8	25	19	9
	Dark	29	26	12	25	20	9	26	21	9
Nearly opaque	Light	42	38	17	36	28	12	38	30	14
	Medium	32	29	13	27	21	9	29	23	10
	Dark	31	28	13	27	21	9	28	22	10

3.2. Temperatures of the Shaded and Sunlit Parts of the Glass at Peak Conditions the Worst Combination of Insulation and Glass Types

The days of occurrence of the highest temperature gradient have been plotted per each location in Figure 6, showing the temperature variation and the relevant daily fluctuation of the direct solar radiation. The combination of glass type and insulation color was "nearly opaque"/"light" for all conditions. Peak values from these days have been used for the sensitivity analysis shown in Appendix A.
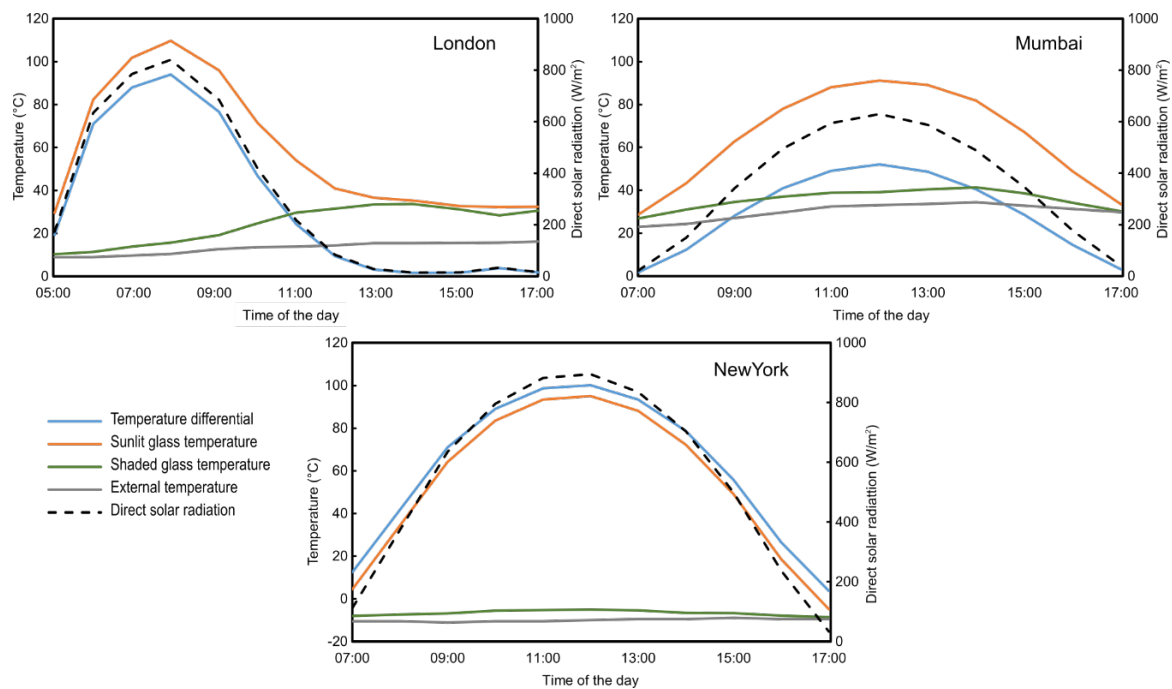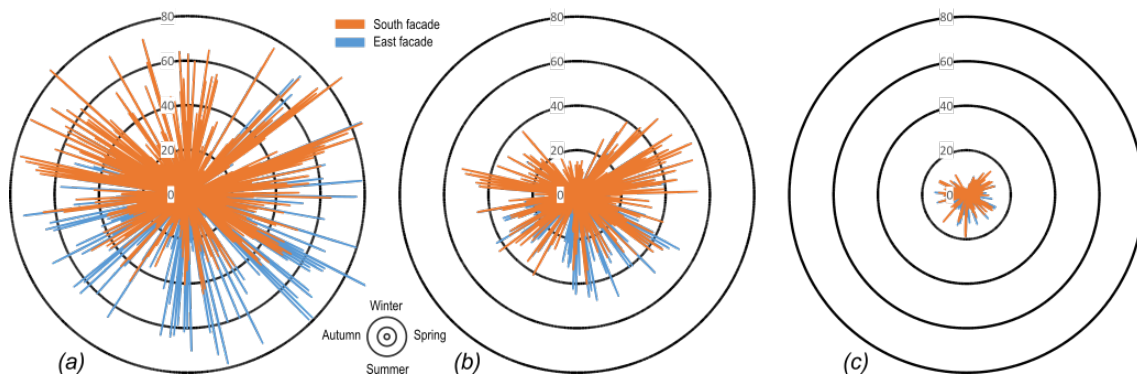
Figure 6. Daily variation of the thermally induced temperature gradients (in Kelvin) for the three analyzed configurations.

3.3. Thermal Stress Variation across the Year for the Worst Combination of Insulation and Glass Types

Figures 7–9 show the yearly variation of the temperature difference for the three locations, the three view angles (0°, 30° and 60°) and two out of three orientations (south and east). The combination of the thermo-physical properties of glass and insulation were the ones leading to the maximum temperature gradient: nearly opaque glass and light insulation color.
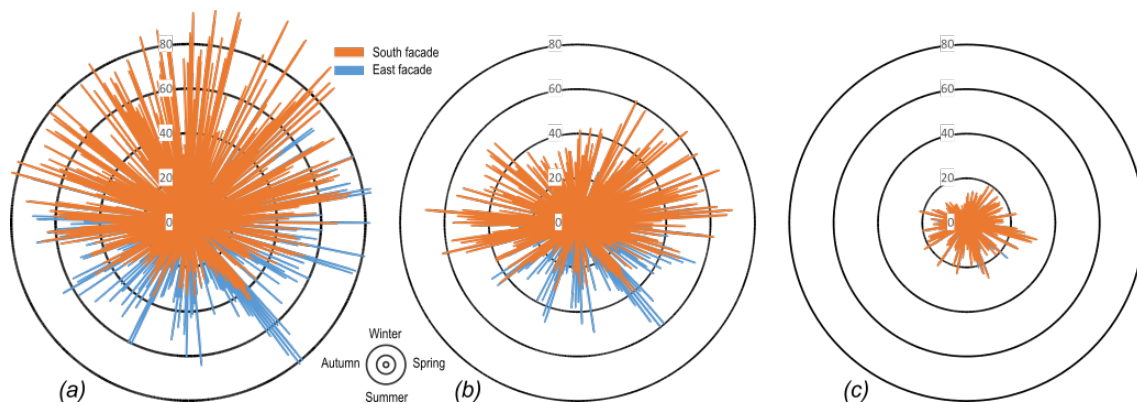
Figure 7. Yearly variation of the thermally induced temperature gradients (K) in New York for values of view angles of 0° (**a**), 30° (**b**) and 60° (**c**) for the worst combination of glass type/insulation type in Tables 5 and 6.

Figure 8. Yearly variation of the thermally induced temperature gradients (K) in London for values of view angles of 0° (**a**), 30° (**b**) and 60° (**c**) for the worst combination of glass type/insulation type in Tables 7 and 8.
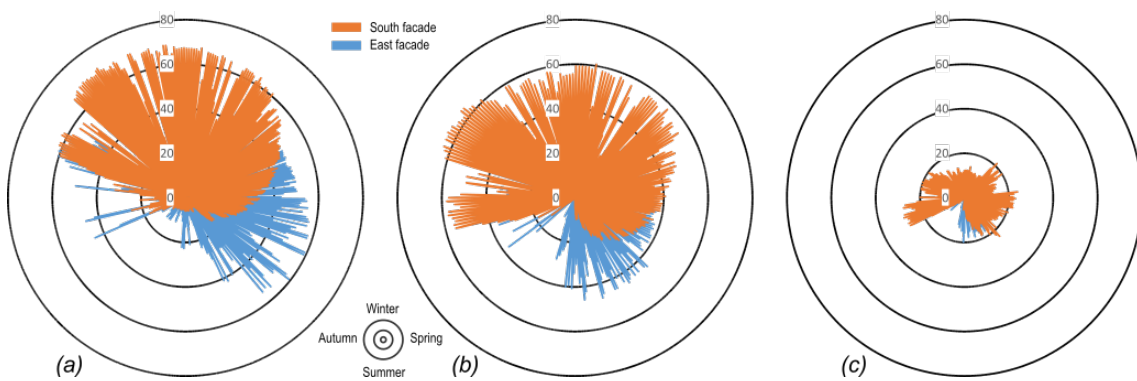
Figure 9. Yearly variation of the thermally induced temperature gradients (K) in Mumbai for values of view angles of 0° (**a**), 30° (**b**) and 60° (**c**) for the worst combination of glass type/insulation type in Tables 9 and 10.

3.4. Incidence of the Thermo-physical Properties of the Spandrel (Step 3)

In step 3, the incidence of the thermo-physical properties of the analyzed spandrel on the temperature gradients was determined. Figure 10 shows, for the three locations, the least-square mean (radius) of the temperature gradients per each level of interaction between glass transparency and insulation absorbance. In each of the diagrams in Figure 10, all values that share the same color are not to be considered statistically different, i.e., the combination of glass transparency/insulation absorptance leads to similar results in the Tuckey post hoc test. In London, all combinations of glass transparency/insulation absorbance resulted in statistically different values except for two combinations: glass transparency equal to 0.4 and insulation absorbance equal to 0.6 and 0.9. In Mumbai, all possible combinations led to statistically different results in terms of temperature gradients ($p < 0.05$). Akin to London, in New York, glass transparency equal to 0.4 with insultation absorbance equal to 0.6 and 0.9 showed predicted means which were not statistically different ($p > 0.05$). The combinations between glass transparency and insulation absorbance, (0.4, 0.6) and (0.4, 0.9), and (0.6, 0.9) and (0.8, 0.9), led to non-statistically different results ($p > 0.05$); all other combinations resulted significantly different from each other.
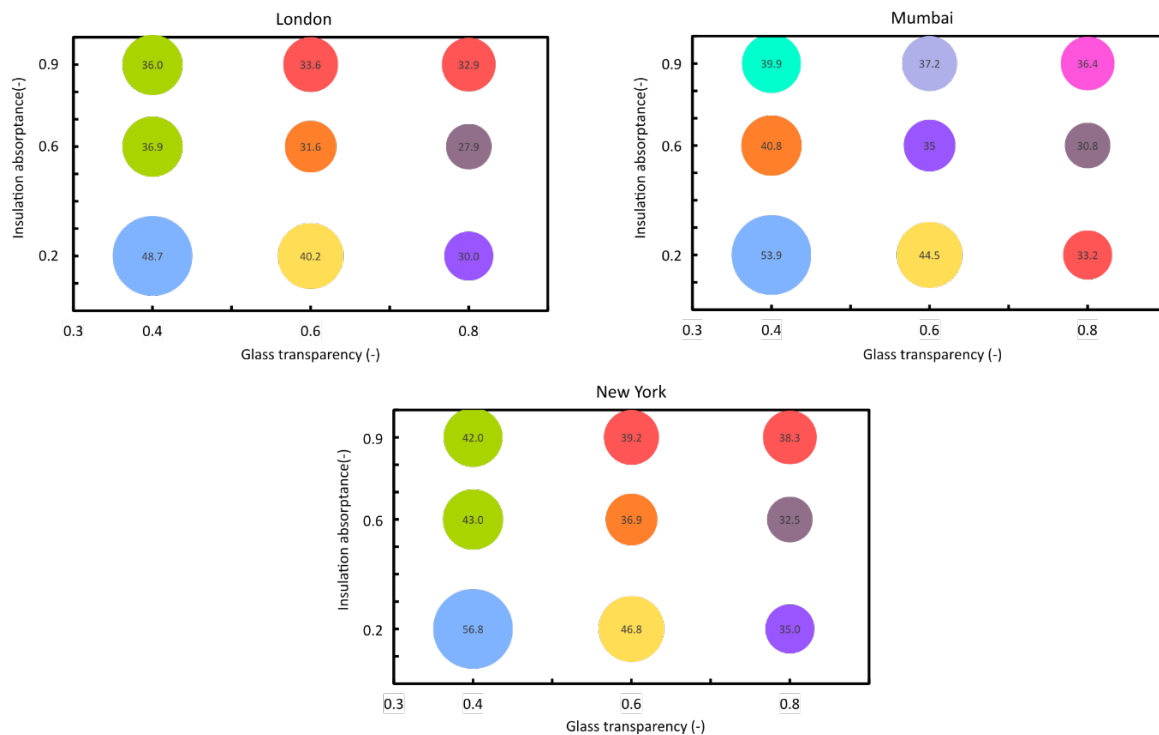
Figure 10. Least square mean (radius of circles) of temperature gradients for the three analyzed locations. Per each location, a combination of variables that leads to results sharing the same circle color means that the combination is not statistically different.

4. Discussion

4.1. Discussion of Results

Results from Tables 5–10 showed specific trends with respect to the selected variables. Understanding the view angle is of fundamental importance, as the solar radiation is reduced by the presence of external shading from the front-facing buildings. On average, reduction rates of 35% and 60% in the maximum temperature gradient were found for view angles of 30° and 60°, respectively, if compared with the 0° case in the three locations analyzed.

The location and the orientation were other important factors governing the phenomenon under investigation, with maximum temperature gradients equal to 100, 94 and 70 K for New York, London and Mumbai, respectively. The peak values for New York and Mumbai took place during winter for south-facing façades, whereas the critical condition for London was during spring for east- and west-facing façades.

Yearly variations showed that south-facing façades in all locations displayed the largest values of temperature gradients in winter, as the direct solar radiation on the vertical plane can reach high values due to the low solar altitudes. East facing façades showed instead larger temperature gradients in spring/summer towards the summer solstice. The role of external shadings from building is fundamental, as the reduction in temperature gradients reduces nearly proportionally to the increase in view angle θ. Hence, it is important to perform accurate solar analysis at early-design stages to evaluate the risk of thermal shock more accurately.

The combination of nearly opaque glass/light insulation color appears to be generally the one leading to the highest temperature gradient. This is also confirmed by the diagrams in Figure 10 that showed how increasing the glass transparency is generally beneficial in reducing such gradient. A dark insulation color (i.e., high absorptance) also made the problem of thermally induced temperature gradients less sensitive to the glass transparency and led to lower values of temperature gradients.

This evidence might be motivated by the fact that the low emissivity of the insulation surface reduces the radiative heat transfer between the insulation and the glass layer.

The Tuckey post hoc analysis showed that most combinations of glass transparency and insulation led to statistically different predicted values of temperature gradients, except for two identical cases in London and New York. In these two locations, fixing the glass transparency to a low value and choosing medium-to-high values of insulation absorptance led to similar results. Similarly, fixing the insulation absorptance at high values and choosing medium-to-high glass transparency led to comparable values of temperature gradients. In Mumbai, despite the low glass transparency/low insulation, absorptance led to the highest value of temperature gradient like in all other locations, and all results were considered statistically different.

Finally, as shown in Appendix A, the value of the thermal resistance of the insulation was not a governing parameter, if it was within reasonable ranges for building applications (e.g., for global U-value compliance).

4.2. Limitations of the Study

The present publication shows a series of limitations, which require further analyses and more insights for subsequent refinements, including model calibration that however falls beyond the scope of this paper. First, although the choice of environmental/thermo-physical variables was aimed at representing the largest spectrum of real-world situations, the number of possible combinations could in fact be larger. For this reason, it is recommended that further studies be conducted. Second, the environmental data were taken from a typical meteorological year (TMY). By default, these values are considered as average for each location. Therefore, indefinable peak conditions (e.g., reflections from the ground) or site-specific peculiarities are not evaluated in this study. Climate change is not considered either, with environmental conditions not considering exceedingly cold or hot days, months or even years. That being the case, and in line with the initial aim of the paper, we recommend not to use the present analyses for code-compliance checking or specific consultancy activities other than initial, early-stage assessment of potential thermally related risks in glasses.

5. Conclusions

The present paper has suggested a methodology for analyzing the thermal shock risk by conducting a three-step process: (1) selection of the hourly environmental conditions, (2) calculation of the detailed temperatures for a widely-used build-up for spandrels in building façades and (3) statistical analysis of the obtained results. The methodology has been applied to different climates, orientations and material properties to identify the underlying factors and trade-offs for material selection to prevent thermal shock risk at early-design stages. The study shows that factors such as climate, orientation and external shading from other buildings govern the risk of thermal breakage. The study further suggests that aesthetically related thermophysical properties of glass and insulation should be carefully selected. This is evidenced by the fact that combining opaque glasses and light insulation colors leads to the highest temperature gradient between sunlit and shaded areas of the glass pane.

Authors would like to recommend this work to be considered by architects, designers, façade engineers and contractors who are interested in understanding how the combination of climate, orientation/shading, and spandrel color may pose a significant risk regarding the occurrence of thermal shock in façades. The paper is thus contributing to support the façade sector in risk mitigation at the early stages of design, which is known to have a prominent role in the final performance and cost of buildings.

Future work will extend the created database by including additional spandrel build-ups (e.g., insulation and double-glazing units) to provide a more direct and user-friendly guidance on the glass specification in terms of required strength.

Appendix A

A spandrel system is normally made of a glazed, externally facing layer and an opaque, highly insulated, internal layer. These two layers are separated by a third, intermediate and sometimes ventilated, air gap. From an energy standpoint, the whole system can be defined as the sum of the thermal resistance of each of the three layers plus the external and internal resistances:

$$R_{tot} = R_{external} + R_{glazed} + R_{air\ gap} + R_{insulation} + R_{internal} \tag{A1}$$

The incidence of the insulation resistance $R_{insulation}$ on the glass temperature gradient was studied by running a sensitivity analysis. The insulation resistance was varied between the minimum and maximum ranges shown in Table A1, by assuming two typically used insulation materials and thicknesses.

Table A1. Variability of the insulation resistance as a function of thickness and material type.

	$R_{insulation}$ for $t_{ins,min}$ = 10 cm (m^{2}K/W)	$R_{insulation}$ for $t_{ins,max}$ = 20 cm (m^{2}K/W)
Polyurethane (λ_{ins} = 0.026 W/mK)	3.8	7.7
Rockwool (λ_{ins} = 0.035 W/mK)	2.9	5.7

The insulation resistance thus varied in the range [2.9, 7.7] m^{2}K/W, with an average value of 5.3 m^{2}K/W. The sensitivity analysis is therefore run by checking how the glass temperature gradient varies with the insulation resistance over three representative instants. Those instants have been chosen to correspond to the peak values already shown in Section 2 and as summarized in Table A2.

Table A2. Environmental parameters and physical properties of the glass at peak conditions of temperature gradients for the analyses conducted in the paper.

	Location	Time of the Day	T_{est} (°C)	I_{dir} (W/m^2)	Glass Type	Insulation Color
Condition 1	New York	12:00 pm	−10.0	894	Nearly opaque	Light
Condition 2	London	8:00 am	10.4	840	Nearly opaque	Light
Condition 3	Mumbai	12:00 pm	33.1	629	Nearly opaque	Light

For each of the three conditions, the three values of insulation resistance [2.9,5.3,7.7] have been used to verify the sensitivity of the problem. Results are shown in Figure A1.
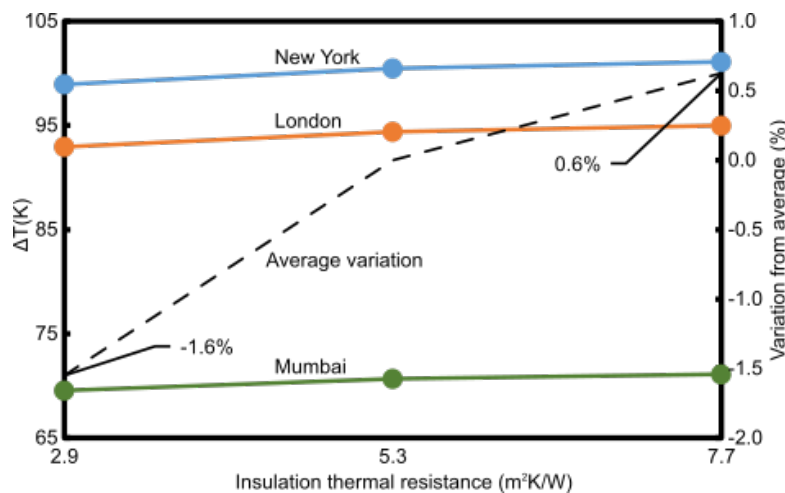
Figure A1. Sensitivity of the problem to the thermal resistance of the insulation.

What emerges is that the problem is weakly sensitive to the variation in insulation resistance, with average variations from the central point (5.3 m^{2}K/W) ranging from −1.6% to 0.6%. Therefore, the insulation thickness can be assumed arbitrarily for the present problem (if it is within "normal" design ranges) since this parameter does not affect results significantly.

References

1. Kassem, M.; Mitchell, D. Bridging the gap between selection decisions of façade systems at the early design phase: Issues, challenges and solutions. *J. Façade Des. Eng.* **2015**, *3*, 165–183. [CrossRef]
2. Montali, J.; Overend, M.; Pelken, P.M.; Sauchelli, M. Knowledge-Based Engineering in the design for manufacture of prefabricated façades: Current gaps and future trends. *Archit. Eng. Des. Manag.* **2017**, *14*, 78–94. [CrossRef]
3. Klein, T. Integral Façade Construction-Towards a New Product Architecture for Curtain Walls. Ph.D. Thesis, Delft University, Delft, The Netherlands, 2013.
4. Voss, E. An Approach to Support the Development of Manufacturable Façade Designs. Ph.D. Thesis, University of Cambridge, Cambridge, UK, 2013.
5. Bergers, M.; Natividad, K.; Morse, S.M.; Norville, H.S. Full scale tests of heat strengthened glass with ceramic frit. *Glas. Struct. Eng.* **2016**, *1*, 261–276. [CrossRef]
6. Dunlap, A.; Asava, R. Three-dimensional condensation risk analysis of insulated curtain wall spandrels. In *Advances in Hygrothermal Performance of Building Envelopes: Materials, Systems and Simulations*; ASTM International: West Kanshohoken, PA, USA, 2017; Volume 1599, pp. 232–260.
7. Behr, R.A. On-site investigations of spandrel glass microenvironments. *Build. Environ.* **1995**, *30*, 61–72. [CrossRef]
8. Triano, J.; Cocca, J. Thermal breakage of spandrel glass: A case study in Forensic Engineering 2012: Gateway to a Better Tomorrow. In Proceedings of the 6th Congress on Forensic Engineering, San Francisco, CA, USA, 31 October–3 November 2012; 2013; pp. 143–150.
9. Jazaeri, J.; Gordon, R.L.; Alpcan, T. Influence of building envelopes, climates, and occupancy patterns on residential HVAC demand. *J. Build. Eng.* **2019**, *22*, 33–47. [CrossRef]
10. Favoino, F.; Overend, M.; Jin, Q. The optimal thermo-optical properties and energy saving potential of adaptive glazing technologies. *Appl. Energy* **2015**, *156*, 1–15. [CrossRef]
11. Ko, M.; Gosti, T.; Kristl, Ž. Influence of architectural building envelope characteristics on energy performance in Central European climatic conditions. *J. Build. Eng.* **2018**, *15*, 278–288.
12. Kültür, S.; Türkeri, N.; Knaack, U. A Holistic Decision Support Tool for Façade Design. *Buildings* **2019**, *9*, 186. [CrossRef]
13. Stamoulis, M.N.; Santos, G.H.; Lenz, W.B.; Tusset, A.M. Genetic Algorithm Applied to Multi-Criteria Selection of Thermal Insulation on Industrial Shed Roof. *Buildings* **2019**, *9*, 238. [CrossRef]

14. Faye, M.; Lartigue, B.; Kane, S. Influence of structural and thermophysical parameters of insulating aggregates on the effective thermal conductivity of lightweight concrete. *J. Build. Eng.* **2019**, *21*, 74–81. [CrossRef]
15. Widiastuti, R.; Caesarendra, W.; Prianto, E.; Budi, W.S. Study on the Leaves Densities as Parameter for Effectiveness of Energy Transfer on the Green Façade. *Buildings* **2018**, *8*, 138. [CrossRef]
16. Widiastuti, R.; Caesarendra, W.; Zaini, J. Observation to Building Thermal Characteristic of Green Façade Model Based on Various Leaves Covered Area. *Buildings* **2019**, *9*, 75. [CrossRef]
17. Tarabieh, K.; Aboulmagd, A. Thermal Performance Evaluation of Common Exterior Residential Wall Types in Egypt. *Buildings* **2019**, *9*, 95. [CrossRef]
18. CSTB, NF DTU P3-Travaux de Bâtiment-Travaux de Vitrerie-Miroiterie-Partie 3: Mémento Calculs des Contraintes Thermiques. 2006. Available online: https://boutique.cstb.fr/39-vitrerie-miroiterie/207-nf-dtu-39-travaux-de-vitrerie-miroiterie-3260050850032.html (accessed on 2 April 2020).
19. *British Standard Institution, BS EN 673-Glass in Building—Determination of Thermal Transmittance (U Value)—Calculation Method*; BSI Standards Publication: London, UK, 2011.
20. Statistical Analysis System Institute. 2019. Available online: https://www.sas.com/en_us/home.html (accessed on 3 April 2020).